Discover Oncology

Research

Analysis of immune infiltration in basal cell carcinoma based on transcriptome sequencing and experimental validation of diagnostic biomarkers

Pengfei Fan[1] · Yun Liu[1] · Tengxiao Ma[1] · Qiaoxing Wang[1] · Lei Li[1]

Received: 3 March 2025 / Accepted: 8 May 2025
Published online: 23 May 2025

Abstract

Background Basal cell carcinoma (BCC) is the most common type of malignant skin tumour, and its incidence is increasing worldwide. While it grows slowly, BCC is locally invasive, causing significant tissue damage. This study investigated the role of mRNAs in BCC through bioinformatics and experimental validation to elucidate the molecular mechanisms involved.

Methods Differentially expressed genes (DEGs) were identified from the transcriptome data of 30 BCC patients and 16 controls from the GSE7553, GSE103439, and GSE42109 datasets. Gene Ontology and KEGG analyses were performed to explore gene expression and pathways. A protein−protein interaction (PPI) network was constructed to identify hub genes, and immune cell infiltration was analysed to study the tumour microenvironment. The diagnostic potential of target genes (LEF1, LGR5, and SOX4) was assessed using ROC curves. Gene expression was validated with qPCR and Western blotting.

Results A total of 135 DEGs were identified, with 9 hub genes selected. LEF1, LGR5, and SOX4 showed strong diagnostic potential, with AUC values of 0.888, 0.955, and 0.996, respectively. The immune cell analysis revealed increased numbers of B cells, NK cells, and T cells in BCC, whereas the numbers of DCs, pDCs, and Treg cells were reduced. qPCR and Western blotting confirmed increased LEF1 and LGR5 expression in BCC. SOX4 expression was increased according to the qPCR results but was not significantly elevated according to the Western blot results, warranting further validation.

Conclusions LEF1, LGR5, and SOX4 may play roles in BCC pathogenesis and could serve as diagnostic biomarkers. These findings provide insights into BCC development and support future research for improved detection and treatment.

Keywords Basal cell carcinoma · Immune infiltration · Diagnostic biomarkers

1 Introduction

Basal cell carcinoma (BCC) is the most common malignant tumour in humans [1, 2], and its incidence has been steadily increasing in recent years. According to the Skin Cancer Foundation, approximately 3.6 million cases are diagnosed annually in the United States alone [3]. The incidence of BCC increases after the age of 40 years and is more common in males [4]. However, due to increasing natural or artificial exposure to ultraviolet (UV) radiation, the incidence in

Pengfei Fan and Yun Liu should be considered joint first author.

✉ Lei Li, ll18638583636@163.com; Pengfei Fan, fpengfei001@163.com; Yun Liu, liuyun1106@sina.com; Tengxiao Ma, mtx_198628@163.com; Qiaoxing Wang, m15120904837@163.com | [1]Department of Plastic and Cosmetic Surgery, Hainan General Hospital, Hainan Affiliated Hospital of Hainan Medical University, Haikou 570311, Hainan, China.

younger populations, particularly in females, has also been increasing [5, 6]. UVB-induced DNA mutations are the most significant risk factor for BCC. Unrepaired DNA damage, including strand breaks and cross-links, can lead to skin cancer through mutations [7]. Furthermore, oxidative stress and UV-induced suppression of antitumour immunity play crucial roles in BCC development [8, 9].

Most BCCs are noninvasive, with metastasis being rare, thus posing a minimal threat to life [10]. However, if left untreated, they can invade and damage surrounding tissues [11]. Standard treatments for BCC include surgical excision or local therapy. In advanced cases, systemic treatments such as Hedgehog pathway inhibitors or immune checkpoint inhibitors may be considered [12]. Nonetheless, both tumour-targeted and immune-targeted therapies are not curative, as most patients experience disease progression following treatment [13]. New therapeutic approaches targeting the tumour microenvironment (TME) are under development and offer promise for improving the management of difficult-to-treat BCC [14]. As such, early diagnosis and personalized treatment strategies remain essential challenges in the clinical management of BCC.

The pathophysiology of BCC involves a complex interaction of genetic factors, sporadic somatic mutations, and environmental influences [15]. One of the most common genetic alterations involved in BCC pathogenesis is dysregulation of the Hedgehog (HH) signalling pathway [16]. The patched receptor (PTCH) is a transmembrane protein that inhibits the HH signalling cascade by suppressing the Smoothened (SMO) protein [16]. Upon binding to HH ligands, PTCH is inactivated, leading to the release of SMO and the activation of glioma-associated oncogene (GLI) proteins. These GLI proteins, upon dissociating from the suppressor of fused (SUFU), translocate to the nucleus, where they act as transcription factors to promote cell proliferation, thereby activating the pathway [16, 17]. Mutations in the HH pathway have been identified in up to 75% of BCC cases, with somatic PTCH1 mutations leading to loss of function and SMO mutations activating the pathway in 10–20% of cases. Less common mutations include loss-of-function alterations in SUFU, a negative regulator of the HH pathway, and mutations in PTCH2, a homologue of PTCH1 [18, 19].

The immune system plays a crucial role in both the initiation and progression of tumours, particularly within the tumour microenvironment (TME). The degree of immune cell infiltration is closely linked to tumour invasiveness, metastatic potential, and the response to treatment [20, 21]. Recent studies suggest that immune cell infiltration not only facilitates tumour immune evasion and resistance but also bidirectionally regulates tumour growth and metastasis [22–24]. In pancreatic ductal adenocarcinoma (PDAC), the immunosuppressive features of the tumor microenvironment are primarily driven by heterogeneous stromal and tumor cells, resulting in limited immune cell infiltration, which contributes to the poor prognosis of PDAC [25]. Recent studies reveal that certain molecular subtypes of breast cancer, particularly HER2-positive and basal-like subtypes, exhibit significant immune infiltration associated with favorable clinical outcomes [26]. Furthermore, research in melanoma demonstrates that tumor cell heterogeneity is closely linked to the distribution of immune cells, with the ratio of CD8 + T cells to regulatory T cells (Tregs) exerting a profound impact on patient survival [27].

Although research on the immune microenvironment of BCC is still relatively limited, the existing studies have highlighted the importance of immune cell infiltration in the pathogenesis of BCC. For example, tumour-infiltrating lymphocytes (TILs) are significantly correlated with the clinical outcomes and prognosis of certain skin cancers [28–30]. Therefore, evaluating the characteristics of immune cell infiltration within the tumour microenvironment, along with investigating immune evasion-related biomarkers, may provide new insights into the early diagnosis and personalized treatment of BCC.

In recent years, the rapid development of high-throughput technologies has made bioinformatics an indispensable tool in cancer research. By analysing gene expression data, researchers can identify key genes and pathways associated with immune cell infiltration, revealing potential molecular biomarkers for cancer diagnosis and prognosis. In the context of BCC, public databases such as Gene Expression Omnibus (GEO) have provided a wealth of gene expression data, facilitating the identification of differentially expressed genes (DEGs) that are closely linked to immune cell infiltration.

This study aims to integrate a bioinformatic analysis with experimental approaches to identify potential diagnostic biomarkers related to immune cell infiltration in BCC. First, gene expression data from BCC samples were analysed through GEO to identify DEGs. A protein—protein interaction (PPI) network and clustering analysis were employed to extract key genes, and their relationships with the immune microenvironment were further examined using immune cell infiltration scoring tools. Second, quantitative PCR (qPCR) and Western blotting (WB) were utilized to validate the candidate genes and explore their roles within the immune microenvironment of BCC, as well as their potential clinical applications. Through this comprehensive approach, we aimed to identify new molecular targets for the early diagnosis of BCC and provide theoretical support for the clinical use of tumour immunotherapy.

2 Materials and methods

2.1 Dataset collection and data preparation

Gene expression data were obtained from the GEO database (https://www.ncbi.nlm.nih.gov/geo/) as of September 8, 2024. Four gene expression profiles were downloaded: GSE7553 [31], GSE103439 [32], GSE42109 [33], and GSE125285 [34]. The training datasets (GSE7553, GSE103439, and GSE42109) used the GPL570 [HG-U133_plus_2] Affymetrix Human Genome U133 Plus 2.0 Array platform for both GSE7553 and GSE103439, whereas GSE42109 utilized both the GPL570 [HG-U133_Plus_2] Affymetrix Human Genome U133 Plus 2.0 Array and the GPL571 [HG-U133A_2] Affymetrix Human Genome U133A 2.0 Array platforms. The validation dataset (GSE125285) was generated using the GPL11154 Illumina HiSeq 2000 (*Homo sapiens*) platform.

The GSE7553 dataset consists of 15 cases of basal cell carcinoma (BCC) and 3 normal skin samples; GSE103439 includes 4 cases of eyelid BCC and 2 normal epidermal keratinocytes; GSE42109 contains 11 cases of BCC and 10 normal skin samples; and GSE125285 includes 25 cases of BCC and 25 normal skin samples. Detailed information is presented in Table 1.

In addition, pathological samples from 3 BCC tissues and 3 adjacent normal tissues during 2024–2025 were enrolled in this study. This study was conducted in accordance with the principles outlined in the Declaration of Helsinki and was approved by the Medical Ethics Committee of Hainan General Hospital.

2.2 Data normalization and identification of DEGs

The raw data were processed using the Affy package, followed by background correction and data normalization to obtain gene expression matrices for the three datasets. The effectiveness of sample correction was visualized in box plots generated with the ggplot2 package [35]. Principal component analysis (PCA) was performed to reduce the dimensionality of the high-dimensional data, and the resulting PCA plot was used to assess sample-to-sample variation. DEGs were identified using the limma[3.52.2] package [36]. A heatmap was generated using the ComplexHeatmap[2.13.1] package [37] to visualize the differential distribution of DEGs. A volcano plot of DEGs was created with the ggplot2[3.3.6] package, applying the criteria of $|\log2FC| > 0.5$ and an adjusted $p < 0.05$(Statistical Power Analysis, Biological Relevance Validation,Field-Standard Alignment, Technical Replicate Verification). A Venn diagram was generated to analyse the common DEGs (co-DEGs) across the three datasets.

2.3 Evaluation of enriched co-DEGs

Functional enrichment analyses of the co-DEGs, including Gene Ontology (GO) and Kyoto Encyclopedia of Genes and Genomes (KEGG) pathway enrichment analyses, were conducted with the clusterProfiler R package. Gene set enrichment analysis (GSEA) was performed to evaluate the distribution trends of genes from a predefined gene set within a ranked gene list based on the phenotype correlation, thereby assessing their contribution to the phenotype. GSEA was conducted separately for each of the three datasets, with a significance threshold set at $P < 0.05$.

Table 1 Dataset collection and data preparation

GEO	Platform	Tissue	Sample (Number)			Experiment type
		(Homo sapiens)	Total	Basal cell carcinoma	Epidermal keratinocytes	
GSE7553	GPL570	Epidermal keratinocytes	18	15	4	Array
GSE103439	GPL570	Epidermal keratinocytes	6	4	2	Array
GSE42109	GPL570 + GPL571	Epidermal keratinocytes	21	11	10	Array
GSE125285	GPL11154	Epidermal keratinocytes	50	25	25	High-throughput sequencing

2.4 PPI network construction and identification of hub co-DEGs

The PPI network for the co-DEGs was constructed using the STRING database (https://www.string-db.org/), and interactions with confidence scores greater than 0.4 were selected. The network was visualized using Cytoscape (V3.9.1), and central genes were further identified using the "CytoHubba" plugin within Cytoscape.

2.5 Analysis of infiltrating immune cells and their functions

Immune cell infiltration analysis: Immune cell scores in tissues were calculated using transcriptomic or other omics data, and algorithms were used to infer the composition of immune cells within the tissue. The single-sample gene set enrichment analysis (ssGSEA) immune cell infiltration algorithm uses specific marker genes for each immune cell type as gene sets to compute the enrichment score for each immune cell type in each sample, thereby inferring immune cell infiltration in individual samples. Given the small sample size, this study employed the "limma" package in R software (version 4.2.1) to merge three expression matrices (GSE7553, GSE103439, and GSE42109) and batch effects were removed using the "sva" package. Immune cell infiltration was calculated via the ssGSEA algorithm provided in the GSVA R package [38], which uses markers for 24 immune cell types, as outlined in the Immunity article [39]. The results were visualized using the ComplexHeatmap (version 2.13.1) package, revealing the correlation between the 24 immune cell types and related functions. P values were compared based on a threshold of 0.05, and correlation plots were generated for values below 0.05.

2.6 Constructing the diagnostic model

Spearman's correlation analysis was performed using the "ggcorrplot" R package to examine the relationships between 9 key co-DEGs, immune cells, and immune functions and to identify potential diagnostic co-DEGs. Three representative feature genes—LEF1, LGR5, and SOX4—were identified as significantly correlated with immune cell infiltration and were selected to predict BCC. A receiver operating characteristic (ROC) curve analysis was conducted using the "pROC" R package (version 1.18.0) to assess the diagnostic performance of these feature genes, with diagnostic efficacy evaluated based on the computed area under the curve (AUC) values. The 3 feature genes were subsequently validated using the GSE125285 dataset.

2.7 Immunohistochemical (IHC) staining

Images of IHC staining normal and basal cell carcinoma samples were downloaded from the Protein Atlas database(HPA, http://www.proteinatlas.org/) and analysed to evaluate hub gene expression at the protein level.

2.8 Quantitative PCR

Total RNA was extracted from tissues using an RNA extraction reagent, chloroform, and isopropanol. The RNA concentration and purity were assessed using a Nanodrop spectrophotometer. Reverse transcription was performed to convert RNA into complementary DNA (cDNA). qPCR was performed with SYBR Green fluorescence dye and specific primers for amplification, with data collected via a PCR instrument. The relative expression of the target gene was calculated using the $2^{-\Delta\Delta CT}$ method. All reagents were purchased from Servicebio (Wuhan) and used according to the manufacturer's instructions. The sequences of all the qPCR primers used in this study are listed in Table 2. Each analysis was performed in triplicate.

2.9 Western blot

Total protein was extracted from tissue samples using RIPA buffer supplemented with protease inhibitors. Protein concentrations were determined using the BCA assay. Equal amounts of protein (30 μg) were separated by SDS—PAGE on a 10% polyacrylamide gel and transferred to PVDF membranes with a semidry transfer system at a constant current of 350 mA for 30 min. The membranes were blocked with 5% nonfat milk in TBST buffer for 1 h and then incubated

Table 2 All the qPCR primers

Primer information	Primer name	Primer sequence (5′–3′)	Fragment length (bp)
NM_003107.3	H-SOX4-S	CTCAAGCACATGGCTGACTACC	135
	H-SOX4-A	ACTGCCACCGACCTTGTCTC	
NM_001277226.2	H-LGR5-S	CTTCCAACCTCAGCGTCTTCA	133
	H-LGR5-A	ATGTATGTCAGAGCGTTTCCCG	
NM_001130714.3	H-LEF1(1) -S	GCGAATGTCGTTGCTGAGTGTA	130
	H-LEF1(1) -A	GCTGTCTTTCTTTCCGTGCTAA	
NM_001101	H-ACTIN-S	CACCCAGCACAATGAAGATCAAGAT	317
	H-ACTIN-A	CCAGTTTTTAAATCCTGAGTCAAGC	

overnight at 4 °C with primary antibodies (anti-LEF1, anti-LGR5, and anti-SOX4, 1:1000; anti-β-actin, 1:5000). After washing, the membranes were incubated with HRP-conjugated secondary antibodies (1:5000) at room temperature for 1 h. The protein bands were detected using ECL reagent and quantified with AIWBwell™ software. The relative expression levels of the target proteins were normalized to those of β-actin.

2.10 Statistical analysis

Data were analysed using R software (version 4.3.3). Student's t test was used to assess the statistical significance of differences between two sets of continuous variables that followed a normal distribution. For continuous variables that did not follow a normal distribution, the Mann–Whitney U test (Wilcoxon rank-sum test) was applied. The chi-square test or Fisher's exact test was used to evaluate the statistical significance of differences between two groups of categorical variables. Pearson's correlation analysis was performed to calculate the correlation coefficients (r) between different genes. A bilateral p value < 0.05 was considered statistically significant. Data from biological triplicate experiments were presented with error bar as mean ± SD. Two-tailed unpaired Student's t-test was used for comparing two groups of data. Statistical signifcance was determined by p-values less than 0.05. The following annotations were used to illustrate signifcance: *$p < 0.05$, **$p < 0.01$, ***$p < 0.001$, and ****$p < 0.0001$.

3 Results

3.1 Data preprocessing and DEG identification

The samples from the three datasets were subjected to combination, balancing, and normalization procedures. The clustering distribution of high-throughput data for the samples was visualized by PCA. After preliminary data processing, all three groups of samples showed a good balance. co-DEGs were visualized in volcano plots and heatmaps. A Venn diagram was constructed to identify the overlap between the three datasets, resulting in the selection of 79 upregulated co-DEGs (Table 3) and 56 downregulated co-DEGs (Table 4), yielding a total of 135 genes (Fig. 1).

3.2 Analysis of the roles and enrichment of co-DEGs

GO and KEGG functional enrichment analyses were performed to analyze the molecular functions of these co-DEGs (Fig. 2A). The results revealed significant enrichment in biological processes such as epithelial tube morphogenesis, epithelial cell proliferation, skin development, the moulting cycle, skin epidermis development, and the canonical Wnt signalling pathway. These biological processes are crucial for normal skin development and homeostasis, and dysregulation of these pathways can contribute to BCC formation. In particular, the canonical Wnt signaling pathway has been implicated in the pathogenesis of BCC, as it plays a key role in regulating cell proliferation, differentiation, and tumorigenesis. Additionally, cellular components, including the collagen-containing extracellular

Table 3 Upregulated co-DEGs

GSE7553 and GSE103439 and GSE42109 upregulated DEGs							
ADAMTS3	VCAN	SOX18	DACT1	SOX11	CNIH3	TFAP2B	COL5A2
LHX2	GAS2	BLM	PLEKHO1	GLI2	MYCN	TRIM9	NAP1L3
KRT85	SYNPO	ARL15	SEMA6A	CRNN	EDIL3	SORL1	TPX2
LPHN3	TM4SF1	DNAJC12	CYFIP2	PAX6	PTCH1	DAPK1	NCAPH
BNC2	HEPH	SDC2	BID	SHOX2	RP11-119F7.5	PSRC1	GINS2
SOX9	PGBD5	BEND5	EFEMP2	SH3GL3	LEF1	STMN1	DNA2
ABI3BP	FARP1	C11orf95	MARCKSL1	DLGAP5	GADD45G	SMARCD3	EMID1
NTRK3	LOXL1	LTBP1	GPC4	VASH2	CACNA2D3	MLLT11	ZNF556
LGR5	S100A9	COL11A1	STON1	CAND2	SOX4	PELI2	NRXN3
MDK	BACH2	AEBP1	RBFOX1	PTPRN2	FZD7	SETBP1	

Table 4 Downregulated co-DEGs

GSE7553 and GSE103439 and GSE42109 downregulated DEGs					
MMP28	C3orf52	GNAI1	HECA	GMPR2	BCL2L13
RNF128	EPAS1	ABCA7	CEBPD	CSPG5	AP1S1
ADRB2	EPPK1	FKBP5	GLUD2	ELOVL5	GDF15
MST1R	SCML1	ISOC2	RETSAT	IRS2	TMEM43
PLCH2	TNS4	SIK1	CRTAP	UBE2I	ECI1
PTPN3	MYC	SLC35F6	GNG12	DALRD3	DNASE2
ECM2	C1orf21	ORAI3	LYST	NKX2-1	
TNNT2	JUN	EML2	NUPR1	RAB9A	
FAS	KLF11	ACP5	STK16	SLC50A1	
SYBU	ARNTL	KLF6	SKAP2	TSPAN14	

matrix and the transcription regulator complex, were enriched. The extracellular matrix (ECM) is critical for tissue architecture and integrity, and alterations in ECM components can facilitate tumor cell migration and invasion, further promoting tumor progression in BCC. The enriched molecular functions included DNA-binding transcription activator activity, RNA polymerase I-specific transcription activator activity, extracellular matrix structural constituent activity, and transcription coregulator binding. These functions suggest that the co-DEGs may contribute to the regulation of gene expression involved in tumorigenesis, particularly by modulating the activity of transcription factors and other regulatory proteins that control cellular behavior in BCC. KEGG pathway analysis revealed that the co-DEGs are closely involved in the biological processes of basal cell carcinoma, highlighting their potential role in its development and progression. Specifically, the activation of signaling pathways such as the Wnt/β-catenin pathway and alterations in ECM components could promote aberrant cell growth and survival, two hallmarks of BCC. Furthermore, dysregulated transcriptional regulation and cell–cell interactions may facilitate the epithelial-to-mesenchymal transition, enhancing the invasive potential of BCC cells. These findings underscore the importance of the identified co-DEGs in the molecular mechanisms underlying BCC pathogenesis.

3.3 Gene set enrichment analysis

GSEA is a widely used bioinformatics method for analysing gene expression data to identify whether specific gene sets are significantly enriched under particular conditions. In this study, we performed GSEA on the GSE7553, GSE103439, and GSE42109 datasets (Fig. 2B–D, Tables 5, 6, 7). The GSEA highlighted the following pathways and processes: REACTOME Cell Cycle Checkpoints, REACTOME DNA Replication, REACTOME Rho GTPases Activate Formins, WP 4249 Hedgehog Signalling Pathway, REACTOME G1/S-Specific Transcription, REACTOME Ion Homeostasis, REACTOME Complement Cascade, WP Electron Transport Chain Oxidative Phosphorylation in Mitochondria, BIOCARTA

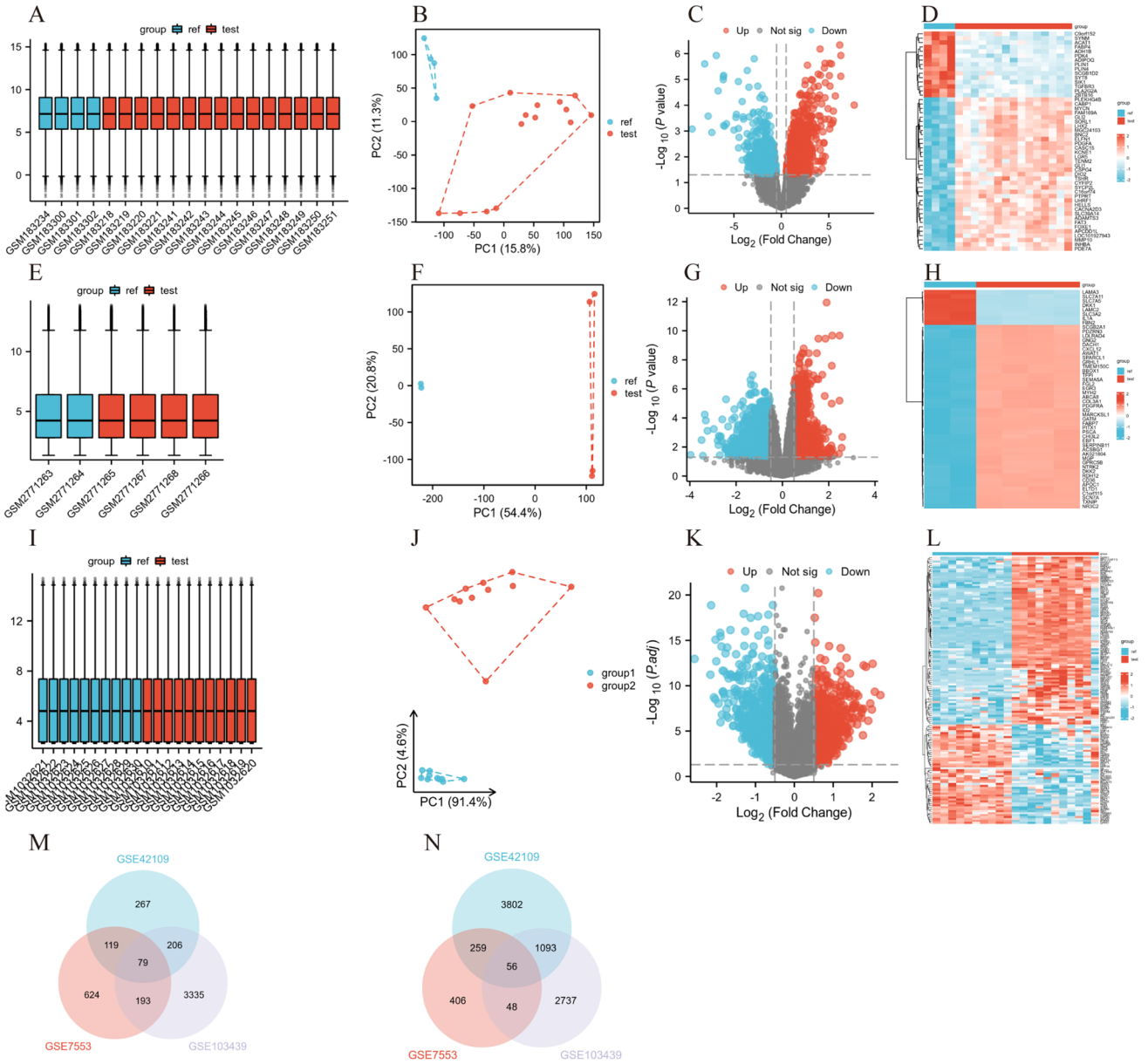

Fig. 1 Data Preprocessing and DEG Identification. **A** Boxplot of the GSE7553 dataset after normalization. **B** PCA of the DEGs between samples of basal cell carcinoma and normal skin in the GSE7553 dataset. **C** Volcano plot of the GSE7553 dataset. **D** Heatmap of the GSE7553 dataset.|log2FC|> 0.5, adj. p < 0.05. **E** Boxplot of the SE103439 dataset after normalization. **F** PCA of the DEGs between samples of basal cell carcinoma and normal skin in the GSE103439 dataset. **G** Volcano plot of the GSE103439 dataset. |log2FC|> 0.5, adj. p < 0.05. **H** Heatmap of the GSE103439 dataset. **I** Boxplot of the GSE42109 dataset after normalization. **J** PCA of the DEGs between samples of basal cell carcinoma and normal skin in the GSE42109 dataset. **K** Volcano plot of the GSE42109 dataset. |log2FC|> 0.5, adj. p < 0.05. **L** Heatmap of the GSE42109 dataset. **M** Venn diagram of the upregulated DEGs. **N** Venn diagram of the downregulated DEGs. **C**, **G**, **K** Red represents the upregulated DEGs; blue represents the downregulated DEGs; grey represents genes with no differential expression. Criteria: |log2FC|> 0.5, adj. p < 0.05

Ghrelin Pathway, KEGG Complement and Coagulation Cascades, REACTOME Regulation of Insulin-like Growth Factor (IGF) Transport and Uptake by IGF-Binding Proteins (IGFBPs), REACTOME Signaling by TGF-β Family Members, KEGG ECM–Receptor Interaction, WP DNA Double-Strand Breaks and Cellular Response via ATM, and KEGG Focal Adhesion. These pathways and processes are implicated in various biological functions, including cell cycle regulation, DNA repair, signal transduction, ion homeostasis, and immune responses, representing the significantly enriched biological pathways identified through GSEA.

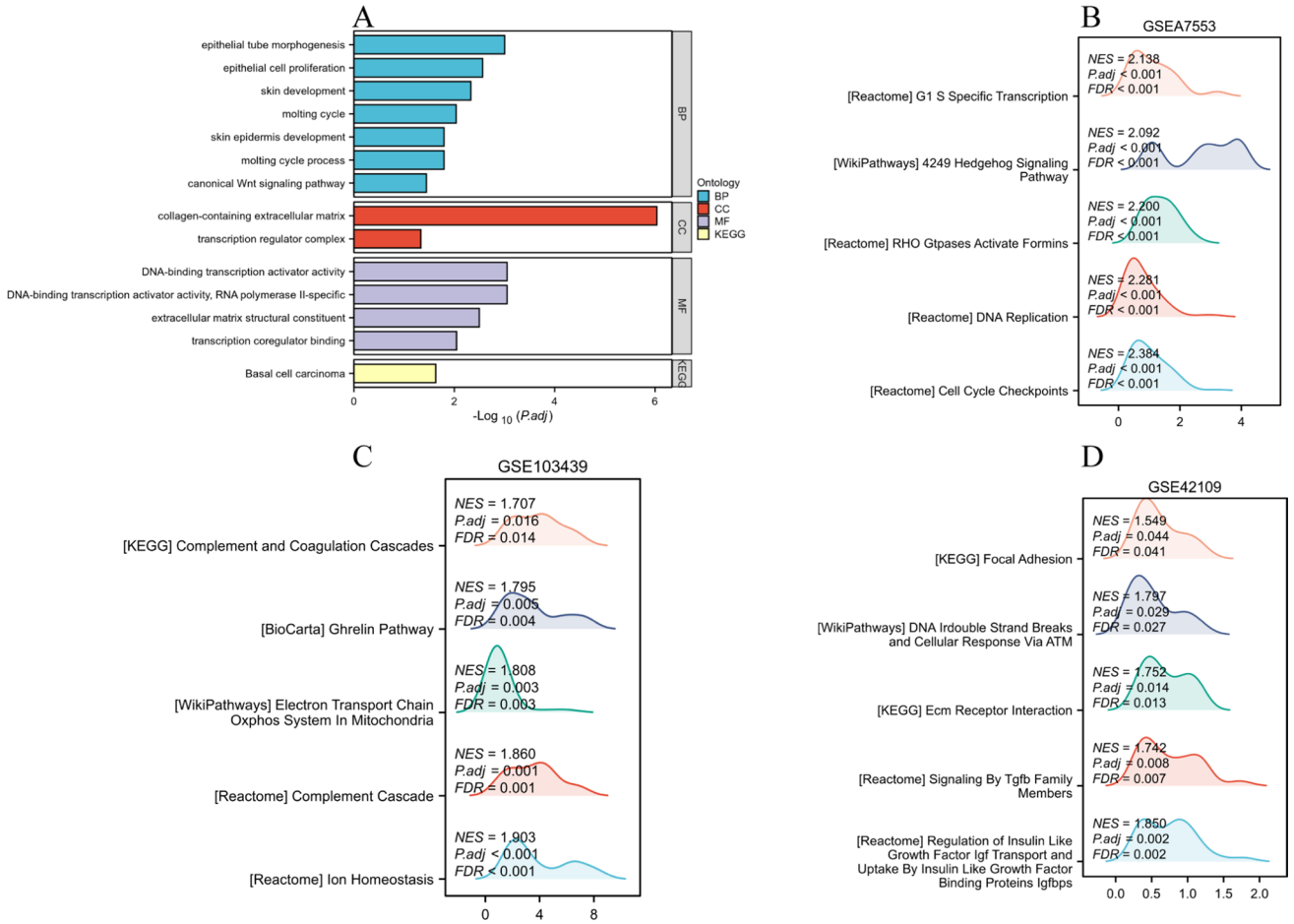

Fig. 2 Enrichment analysis. **A** GO and KEGG functional enrichment analyses of the co-DEGs. **B** GSE7553 GSEA.adj. $p < 0.05$. **C** GSE103439 GSEA.adj. $p < 0.05$. **D** GSE42109 GSEA.adj. $p < 0.05$

Table 5 GSE7553 GSEA

ID	Enrichment Score	NES	p.adjust	Rank
REACTOME_CELL_CYCLE_CHECKPOINTS	0.548307018	2.3839002	4.13E-08	4236
REACTOME_DNA_REPLICATION	0.569719773	2.280868579	2.61E-07	5375
REACTOME_RHO_GTPASES_ACTIVATE_FORMINS	0.543904514	2.200439215	2.12E-06	2190
WP_4249_HEDGEHOG_SIGNALING_PATHWAY	0.645551817	2.091570592	0.000906854	1253
REACTOME_G1_S_SPECIFIC_TRANSCRIPTION	0.706220451	2.138417818	0.000918911	4053

Table 6 GSE103439 GSEA

ID	Enrichment Score	NES	p.adjust	Rank
REACTOME_ION_HOMEOSTASIS	0.735765998	1.902579425	0.0004582	1525
REACTOME_COMPLEMENT_CASCADE	0.709104854	1.859817725	0.001327734	2141
WP_ELECTRON_TRANSPORT_CHAIN_OXPHOS_SYSTEM_IN_MITOCHONDRIA	0.663891425	1.807765916	0.003063468	4379
BIOCARTA_GHRELIN_PATHWAY	0.877426567	1.795126009	0.004720503	1744
KEGG_COMPLEMENT_AND_COAGULATION_CASCADES	0.637239803	1.706683802	0.016085398	1629

Table 7 GSE42109 GSEA

ID	Enrichment Score	NES	p.adjust	Rank
REACTOME_REGULATION_OF_INSULIN_LIKE_GROWTH_FACTOR_IGF_TRANSPORT_AND_UPTAKE_BY_INSULIN_LIKE_GROWTH_FACTOR_BINDING_PROTEINS_IGFBPS	0.579398295	1.849937608	0.00177198	1265
REACTOME_SIGNALING_BY_TGFB_FAMILY_MEMBERS	0.533694848	1.742356754	0.007867701	1194
KEGG_ECM_RECEPTOR_INTERACTION	0.570994895	1.752008102	0.014229984	1103
WP_DNA_IRDOUBLE_STRAND_BREAKS_AND_CELLULAR_RESPONSE_VIA_ATM	0.632346149	1.796539106	0.028966336	2120
KEGG_FOCAL_ADHESION	0.449107121	1.549375882	0.044006151	1447

3.4 Analysis of PPI networks

We analysed PPIs among the co-DEGs using the STRING database (https://www.string-db.org/). MCODE was utilized to identify hub genes (Fig. 3A), whereas CytoHubba, which employs the MCC, degree, and MNC algorithms, was applied to predict the top 10 target genes (Fig. 3B–D). A total of 9 overlapping genes were identified across the three algorithms: MYC, JUN, SOX9, LEF1, GLI2, LGR5, SOX4, PAX6, and MYCN. A Venn diagram illustrating the hub genes was also generated (Fig. 3E).

3.5 Analysis of hub genes

A heatmap of the hub genes is presented in Fig. 4A. The expression of the hub genes MYC, JUN, SOX9, LEF1, GLI2, LGR5, SOX4, PAX6, and MYCN in GSE125285 was analysed (Fig. 4B). The differential expression of these genes between the disease and control groups was compared. The expression levels of MYC, JUN, SOX9, LEF1, GLI2, LGR5, SOX4, PAX6, and

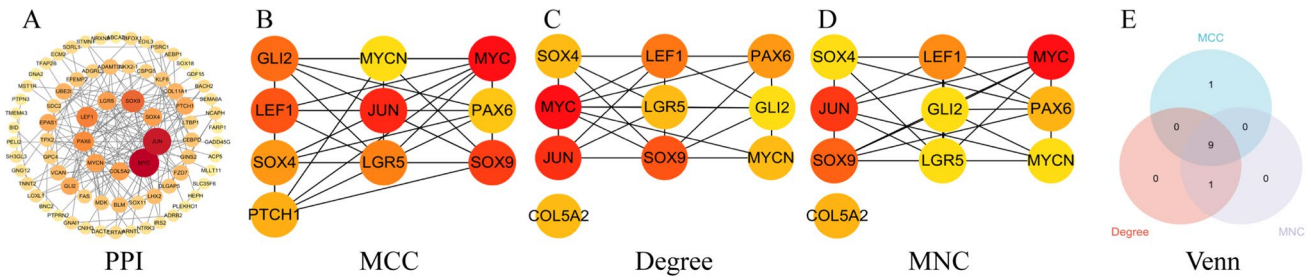

Fig. 3 Protein−protein interaction network analysis of the co-DEGs. **A** The PPI network. **B** Prediction of the MCC. **C** Prediction of the degree. **D** Prediction of the MNC. **E** Combined results obtained from using the three algorithms. Hub gene prediction is shown as a gradual change from yellow to red, and the darker the red is, the higher the accuracy of the prediction

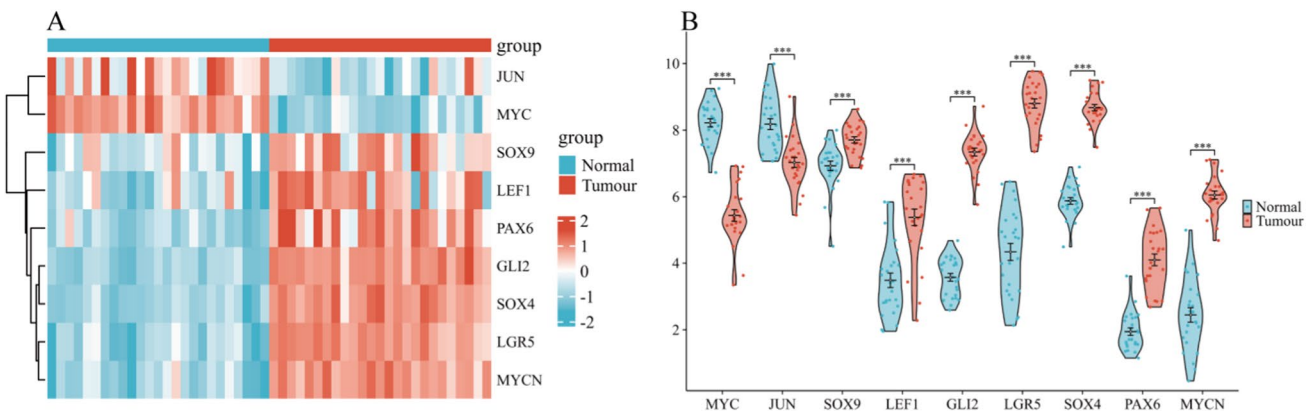

Fig. 4 Analysis of the expression of the hub genes in GSE125285

MYCN were significantly different ($p < 0.001$). Specifically, MYC and JUN were downregulated in BCC, whereas SOX9, LEF1, GLI2, LGR5, SOX4, PAX6, and MYCN were upregulated in BCC. A Mann−Whitney U test (Wilcoxon rank-sum test) was performed, with *$p < 0.05$, **$p < 0.01$, and ***$p < 0.001$ indicating statistical significance.

3.6 Analysis of infiltrating immune cells and their functions

An analysis of immune cell infiltration is a key method in cancer research and focuses on examining immune cell infiltration in the tumour microenvironment to understand its role in tumour initiation, progression, and the response to treatment. This analysis provides valuable insights into tumour immune microenvironments, aids in determining the prognosis of cancer, and supports the development of immune-based therapies and novel drug discovery. With ongoing advancements in analytical technologies, an immune cell infiltration analysis is poised to play an increasingly critical role in both research and clinical practice.

We integrated three datasets and standardized the data to further investigate immune cell infiltration and function in BCC patients compared with normal controls (Fig. 5A). Using ssGSEA, we assessed the enrichment scores of various immune cell subpopulations and functions. The results are presented in a heatmap (Fig. 5B) and box plot (Fig. 5C). In BCC tissues, the numbers of B cells, NK CD56bright cells, T cells, TFH cells, Th1 cells, and Th2 cells were increased, whereas the numbers of DCs, pDCs, and Treg cells were decreased. NS indicates no statistical significance; *$p < 0.05$, **$p < 0.01$, and ***$p < 0.001$ indicate statistical significance.

3.7 Diagnostic model

We analysed the correlations between the expression of three hub genes (LEF1, LGR5, and SOX4), immune cells, and immune functions to identify potential diagnostic biomarkers for BCC. Based on this analysis, we selected these three immune cell infiltration-related hub genes as candidate diagnostic markers for BCC. The diagnostic performance of this gene-based model was evaluated using the a ROC curve analysis. The predictive model was validated using the GSE125285 dataset. The results indicated that these three genes exhibit promising predictive value for BCC. However, the accuracy and reliability of this diagnostic model still need to be further assessed in future clinical trials (Fig. 6).

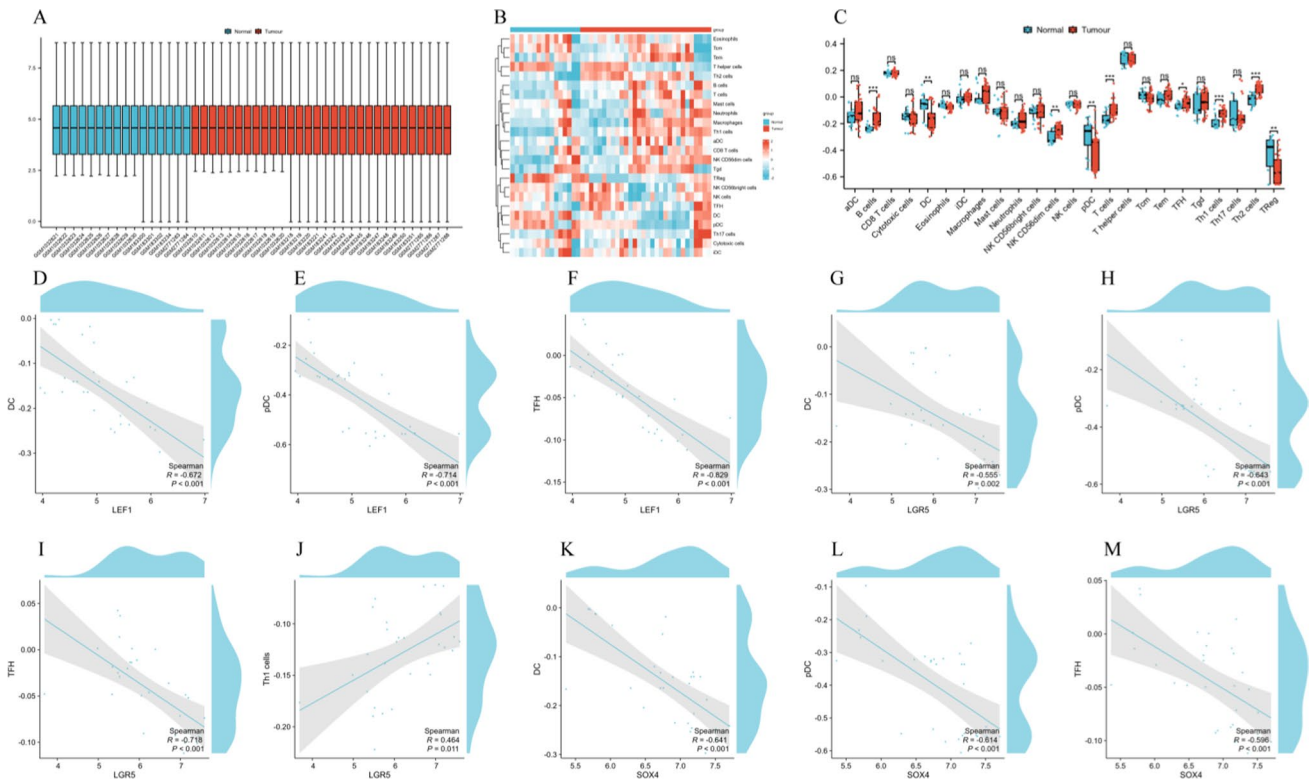

Fig. 5 Infiltration analysis of immune cells. Relationships between HUB genes and immune cells. **D**–**F** LEF1. **L**–**J** LGR5. **K**–**M** SOX4

3.8 Expression of the three hub genes across cancers and basal cell carcinoma tissues

First, we used the Kaplan−Meier plotter to examine the expression of the three hub genes across various normal and tumour tissues. The pancancer analysis revealed higher expression levels of LEF1, LGR5, and SOX4 in most tumour tissues than in normal tissues. Additionally, through the Protein Atlas database (https://www.proteinatlas.org/), we confirmed the expression of LEF1, LGR5, and SOX4. Images of IHC staining were downloaded from the HPA database to evaluate the expression of the hub genes (LEF1, LGR5 and SOX4) at the protein level. As shown in Fig. 7, normal skin had negative IHC staining, whereas tumour tissues displayed moderate staining. Furthermore, we also noted that these genes were highly expressed in other tumour tissues, such as lung cancer and colorectal cancer (not shown). Therefore, these hub genes may be involved in the development of several tumours, which is consistent with the results of our previous bioinformatic analysis (Fig. 7).

LEF1 protein expression was greater in BCC tissue than in normal tissue. LGR5 protein expression was greater in BCC tissue than in normal tissue. SOX4 protein expression was greater in BCC cancer tissue than in normal tissue.

3.9 Expression of the three hub genes in BCC

We further validated the expression of LEF1, LGR5, and SOX4 in BCC using qPCR, which confirmed the elevated expression levels of these genes in BCC tissues (Fig. 8A), and the differences were statistically significant ($P < 0.05$). We subsequently conducted Western blot experiments and compared the protein expression levels between BCC tissues and adjacent normal tissues. The results revealed significantly higher expression levels of LEF1 and LGR5 in BCC tissues than in adjacent normal tissues ($P < 0.05$). However, although the SOX4 protein level was higher in BCC tissues than in adjacent normal tissues, the difference was not statistically significant ($P > 0.05$) (Fig. 8B–F). These findings collectively suggest that LEF1, LGR5, and SOX4 may play a tumour-promoting role in basal cell carcinoma.

4 Discussion

Basal cell carcinoma is the most common type of skin cancer in humans and is triggered primarily by UV radiation. BCC usually appears on the head and face, with its incidence increasing annually. Although the pathogenesis of BCC is not yet fully understood, advanced BCC can cause significant destruction of soft tissues, cartilage, and even bone, leading to severe disfigurement and functional impairments, and thus imposing a substantial global health and economic burden [40, 41]. The development of BCC is associated mainly with mutations in the HH signalling pathway, and SMO inhibitors have been approved for the treatment of locally advanced and metastatic BCC [42]. However, significant side effects, poor drug tolerance, and resistance in SMO mutation subtypes necessitate further exploration of the molecular mechanisms of BCC. This research is crucial for identifying more effective treatment targets. In this study, we analysed the GSE7553, GSE103439, and GSE42109 datasets, and validated our findings with the GSE125285 dataset. Through data mining, 135 co-DEGs were identified. GO and KEGG functional enrichment analyses were subsequently performed, and through an analysis of the PPI network, nine key hub genes (MYC, JUN, SOX9, LEF1, GLI2, LGR5, SOX4, PAX6, and MYCN) were identified. Among these genes, LEF1, LGR5, and SOX4 were the most representative hub genes, and their roles in BCC were further explored. A diagnostic model was constructed to assess the predictive ability of these three hub genes, and immune cell infiltration was analysed to explore the tumour microenvironment of BCC.

We collected three BCC tissue samples and three adjacent normal tissue samples for qPCR experiments to verify the changes in gene expression, ensuring the reliability of our results. The ROC curve analysis revealed that LEF1, LGR5, and SOX4 expression in BCC patients effectively predicted disease presence. The AUC values for LEF1, LGR5, and SOX4 were 0.888, 0.955, and 0.996, respectively (Fig. 6), indicating that these genes accurately differentiated BCC patients from healthy individuals. Further analysis revealed that these genes are significantly expressed in other cancer types and are classified as oncogenes. Therefore, we propose that LEF1, LGR5, and SOX4 expression may serve as novel biomarkers for BCC.

ssGSEA indicated that BCC tissues contained increased numbers of B cells, T cells, T follicular helper (TFH) cells, Th1 cells, Th2 cells, and NK CD56bright cells. In contrast, the levels of dendritic cells (DCs), plasmacytoid dendritic cells (pDCs), and regulatory T cells (Tregs) were lower. In the gene–immune cell correlation analysis, LEF1 and SOX4

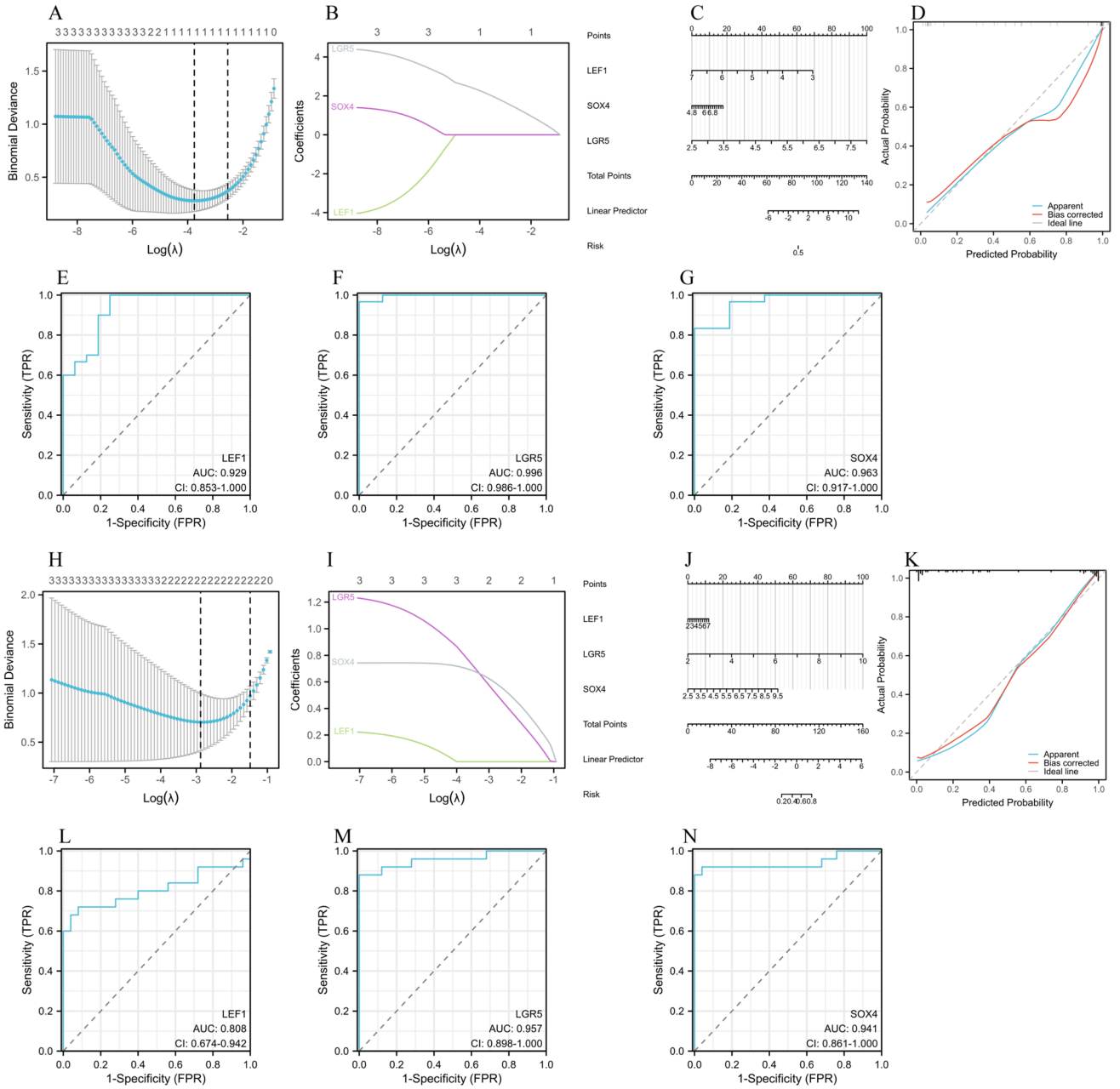

Fig. 6 Screening of basal cell carcinoma hub genes and evaluation of their diagnostic value. **A**–**F** Experimental Set. **A**, **B** LASSO analysis for screening basal cell carcinoma hub genes. **C** Identification of the hub genes according to the importance of the variables by random forest (RF) analysis of the hub genes. **D** Calibration curves of the BCC risk models. **E**–**G** ROC curves of the four hub genes used to assess their diagnostic value in the Experimental Set. **H**–**N** Validation Set. **H**, **I** LASSO analysis for screening basal cell carcinoma hub genes. **J** Identification of the hub genes according to the importance of the variables by random forest (RF) analysis of the hub genes. **K**. Calibration curves of the BCC risk models. **L**–**N** ROC curves of the four hub genes used to assess their diagnostic value in the Validation Set. Calibration curves **D**, **K**: The x-axis represents the predicted survival probability of the model, and the y-axis represents the actual observed survival probability. The Apparent curve represents the predicted curve, the Bias-corrected curve represents the calibration curve, and the Ideal curve represents the ideal curve. The closer the curves are to the diagonal line, the better the fit. The distribution plot at the top of the graph shows the distribution of predicted probabilities. The more concentrated the distribution, the more samples fall within that probability.The ROC curve **E**–**G**, **L**–**N** is a graphical representation of the relationship between sensitivity and specificity. The x-axis represents 1—specificity, also known as the false positive rate; the closer the x-axis is to zero, the higher the accuracy. The y-axis represents sensitivity, also known as the true positive rate; the higher the y-axis, the better the accuracy. The area under the AUC is commonly used to evaluate diagnostic tests. The AUC value typically ranges from 0.5 to 1, with a higher AUC (closer to 1) indicating better diagnostic performance of the variable in predicting outcomes. The optimal cutoff value of the ROC curve is the point where the sum of the false positive rate and false negative rate is minimized. The Youden index is often used to determine the best cutoff value, calculated as Youden index = (sensitivity + specificity)—1

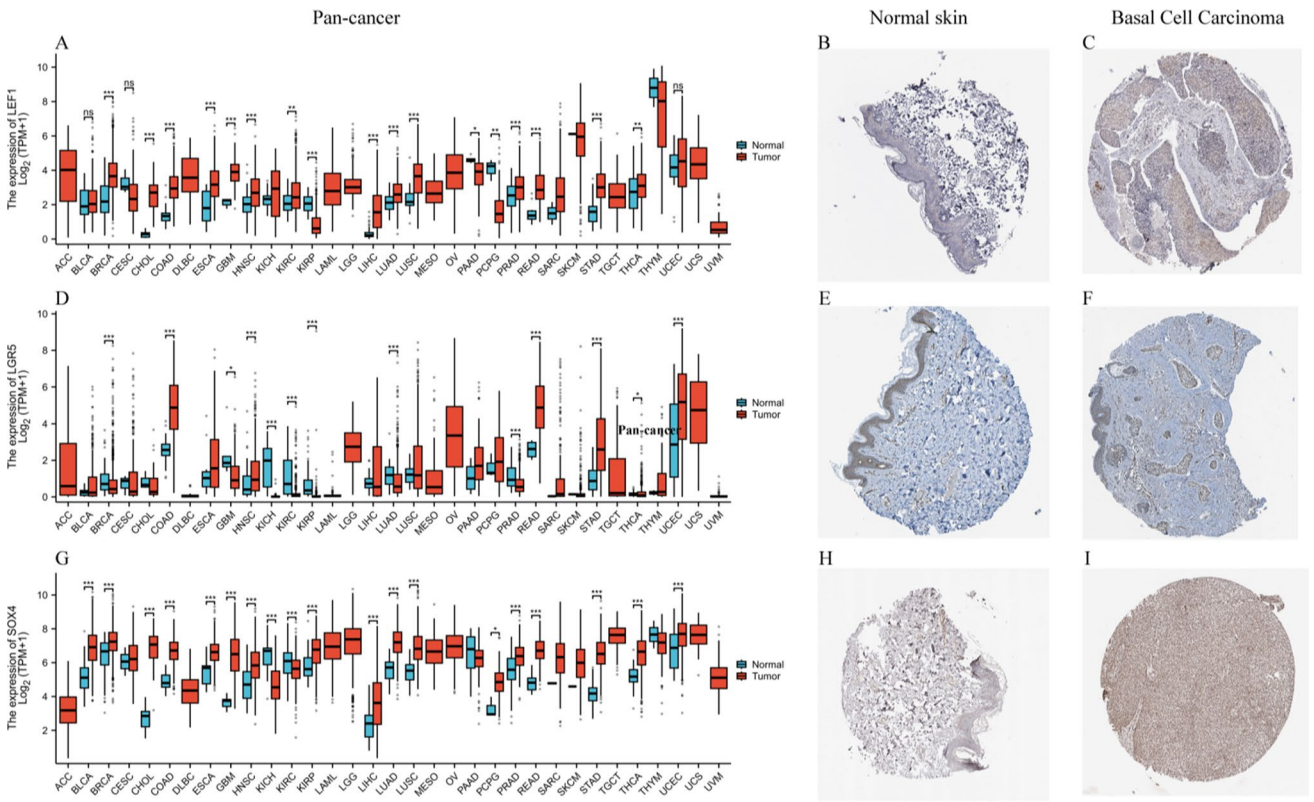

Fig. 7 Expression of the three hub genes in pancancer and BCC samples. **A**, **D**, **G** Expression of the three hub genes in the pancancer samples. **B**, **C**, **E**, **F**, **H**, **I** Images of normal and basal cell carcinoma tissues extracted from the HPA (http://www.proteinatlas.org/) immunostained for the hub genes. **B** Anti-LEF1 Antibody HPA002087, Female, age 4, Skin (T-01000),Normal tissue, Patient id: 1704, **C** Anti-LEF1 Antibody HPA002087, Female, age 57, Skin (T-01000), Basal cell carcinoma (M-80903), Patient id: 2554, **E** Anti-LGR5 Antibody HPA012530, Female, age 41, Skin (T-01000), Normal tissue, Patient id: 2956, **F** Anti-LGR5 Antibody HPA012530, Female, age 84, Skin (T-01000), Basal cell carcinoma (M-80903), Patient id: 1942, **H** Anti-SOX4 Antibody HPA029901, Female, age 17, Skin (T-01000), Normal tissue, Patient id: 3532; **I** Anti-SOX4 Antibody HPA029901, Female, age 84, Skin (T-01000), Basal cell carcinoma (M-80903), Patient id: 1983

expression were negatively correlated with DCs, pDCs, and Treg cells, whereas LGR5 expression was negatively correlated with DCs, pDCs, Tregs, and Th1 cells. These changes in immune cell populations can be analysed in terms of immune activation and immune escape. The increased number of immune cells suggests an enhanced immune response in BCC tissues. This phenomenon is particularly evident in the activation of T cells (Th1, Th2, and TFH) and B cells, which may play significant roles in the immune response to BCC. The increase in the number of NK CD56bright cells might be related to immune surveillance and cytotoxic activity against tumour cells. The decreases in the numbers of DCs, pDCs, and Treg cells may indicate that tumour cells suppress immune activation or antigen presentation, weakening the effectiveness of the immune response. DCs and pDCs are important antigen-presenting cells, and reductions in their numbers may impair the initiation of immune responses. The reduction in the number of Treg cells could be associated with immune escape mechanisms, as Treg cells typically suppress excessive immune responses to prevent autoimmune attacks, and the decrease in their numbers may diminish the ability of tumours to escape the immune system. The analysis of gene expression patterns and immune cell data suggested that the immune microenvironment in BCC likely exhibits some degree of immune evasion. The reductions in the numbers of DCs and Treg cells could assist tumours in evading immune detection and attack. High levels of LEF1, LGR5, and SOX4 may change the composition of immune cells, promoting tumour growth and helping tumours evade the immune system. This process occurs mainly by inhibiting the functions of DCs and Treg cells, which exacerbate immunosuppression. In summary, the immune microenvironment in BCC appears to use mechanisms of immune escape to avoid clearance by the immune system. This process is accomplished by increasing the numbers of certain immune cells, such as B cells and T cells, while suppressing the functions of DCs, pDCs, and Treg cells, thus reducing the effectiveness of the immune system. These findings suggest a complex immune cell and gene expression pattern in BCC, with

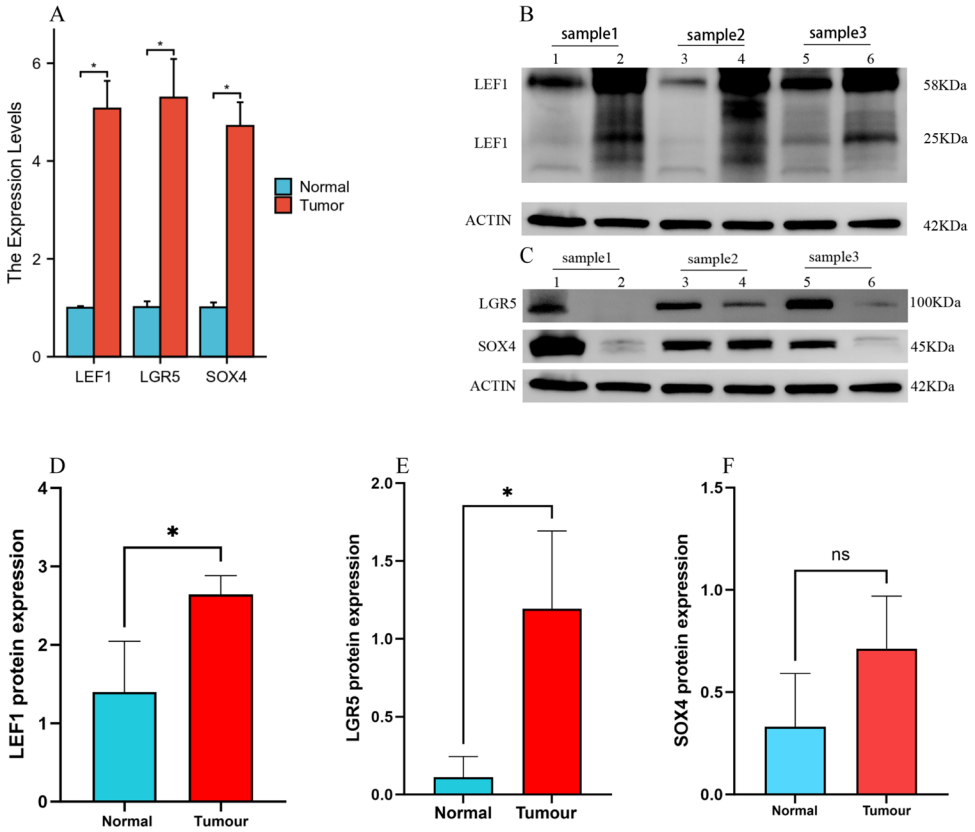

Fig. 8 Expression of the three hub genes in BCC. **A** The expression levels of LEF1, LGR5, and SOX4 were measured in basal cell carcinoma tissues using qPCR analysis. **B**, **C** The expression levels of the same genes were measured in BCC tissues using Western blot analysis. **D**–**F** We compared the protein expression levels of LEF1, LGR5, and SOX4 in BCC tissues with those in adjacent normal tissues. (NS indicates no statistical significance. *$p < 0.05$, **$p < 0.01$, and ***$p < 0.001$. In Figure B, Panels 1, 3, and 5 show adjacent normal tissues, whereas Panels 2, 4, and 6 show BCC tissues. In Figure C, Panels 1, 3, and 5 display BCC tissues, whereas Panels 2, 4, and 6 display adjacent normal tissues

the upregulation of LEF1, LGR5, and SOX4 closely linked to these immune changes. Interventions targeting these changes may provide new strategies for immunotherapy and targeted therapy for BCC.

qPCR was conducted on three samples to validate the experimental results. The statistical analysis revealed that the expression levels of target genes in BCC tissues were significantly higher than those in adjacent normal tissues, with $P < 0.05$ indicating statistical significance. Subsequent Western blot experiments confirmed the expression of these genes at the protein level, providing additional insights into their potential roles in BCC. The results showed that the expression of LEF1 in BCC tissues was significantly higher than that in adjacent normal tissues, suggesting that LEF1 may play an important regulatory role in BCC. LEF1 is a downstream transcription factor in the Wnt/β-catenin signalling pathway and plays a crucial role in the development and progression of various cancers. Research indicates that abnormal LEF1 expression is linked to tumour invasiveness, metastasis, and patient prognosis. Recent studies have focused on the role of LEF1 in different cancer types. For example, in colon cancer, high LEF1 expression closely correlates with the proliferation and migratory capabilities of tumour cells. In ovarian cancer, the long noncoding RNA LEF1-AS1 promotes tumour progression through interactions with miR-1285-3p, and its expression level is positively correlated with lymph node metastasis and the tumour stage [43, 44]. Additionally, LEF1 regulates androgen receptor expression and promotes prostate cancer cell growth and invasion [45]. In breast cancer, LEF1 expression is associated with tumour invasiveness, particularly in tumours lacking ErbB2 overexpression [46]. Recent studies have suggested that LEF1 may contribute to cancer metastasis and drug resistance through multiple molecular mechanisms. For example, the interaction between LEF1 and miR-34a plays a key role in the epithelial—mesenchymal transition (EMT) in prostate cancer, affecting cancer cell migration and invasion [47–49]. LEF1 can also regulate the Wnt/β-catenin signalling pathway, influencing cancer cell growth and survival [44].

Our pancancer analysis revealed markedly increased LGR5 gene expression in several specific cancer types (Fig. 7D). LGR5 is a key stem cell marker that plays a critical role in various cancers. Recent studies have shown that LGR5 not only maintains intestinal stem cells but also participates in cancer development and progression. LGR5 overexpression is correlated with a poor prognosis for multiple cancer types, including colorectal, gastric, and pancreatic cancers. In colorectal cancer (CRC), LGR5 expression is closely related to tumour invasiveness and metastatic potential. Studies have shown that LGR5-positive cells possess self-renewal and differentiation capabilities, endowing them with a dominant position in the tumour microenvironment. Treatments targeting LGR5 have been shown to effectively inhibit the growth and metastasis of colorectal cancer cells in mouse models. For example, studies have shown that LGR5-targeting antibody—drug conjugates

(ADCs) significantly reduce the tumour burden in mouse models [50, 51]. Additionally, LGR5 is considered a cancer stem cell marker and is involved in drug resistance and tumour recurrence. Research indicates that LGR5-positive cells have a higher survival rate after chemotherapy, suggesting their critical role in tumour relapse. Targeting LGR5 has emerged as a potential strategy to overcome current drug resistance issues in cancer therapy. In gastric cancer, LGR5 expression is also associated with chemotherapy resistance. Studies have shown that gastric cancer patients with high LGR5 expression have poorer chemotherapy responses and prognoses. RNA interference targeting LGR5 increases the sensitivity of gastric cancer cells to chemotherapy drugs [52]. Furthermore, the WB analysis revealed significantly higher LGR5 expression in BCC tissues than in adjacent normal tissues, suggesting that LGR5 may participate in the progression and malignant transformation of BCC. These results indicate that LGR5 could serve as a potential biomarker or therapeutic target for BCC, warranting further investigation in future studies. Our pancancer analysis revealed that the SOX4 gene was significantly overexpressed in various cancers. However, Western blot analyses revealed that although SOX4 expression in BCC tissues was higher than that in adjacent normal tissues, the difference did not reach statistical significance. This discrepancy may be due to low SOX4 protein expression, a small sample size, or issues with antibody sensitivity. The incomplete concordance between SOX4 transcriptional levels and protein expression may arise from post-transcriptional regulation [53], temporal kinetic disparities, and methodological variables, but may also reflect that this molecule serves as a critical node in dynamic regulatory networks during basal cell carcinoma progression [53].

The negative correlation between LEF1/SOX4 and DC infiltration suggests: Wnt/β-catenin signaling (via LEF1) and SOX4-mediated epigenetic silencing (e.g., downregulation of FLT3L, a DC survival factor) may suppress DC recruitment/maturation. Reduced DCs/pDCs (validated by ssGSEA) likely impair tumor antigen presentation to CD8 + T cells, enabling immune escape [54]. While Treg depletion typically enhances antitumor immunity, its reduction in BCC may reflect: Th2 cytokine dominance (e.g., IL-4/IL-13) driving M2 macrophage polarization to maintain immunosuppression [55, 56] LGR5 + cancer stem cell (CSC)-secreted TGF-β/IL-10 directly inhibiting Treg differentiation while inducing T-cell exhaustion [57]. BCC-elevated TGF-β (associated with LEF1/SOX4) correlates with: Impaired NK cell cytotoxicity and IFN-γ production via SMAD3-dependent pathways [58–60]. LEF1 activation suppresses DC/T-cell chemoattractants (CCL4/CCL5) while upregulating PD-L1 [61–63]. LGR5 + CSCs may secrete apoptosis-inducing factors (e.g., TRAIL) for DC elimination and promote Breg-mediated CD8 + T-cell suppression.

This finding could also suggest that the role of SOX4 in BCC is more indirect or that its expression is heterogeneous. Overall, the high expression of LEF1 and LGR5 in BCC supports their potential roles in tumorigenesis, whereas the role of SOX4 may be more limited. Future studies should optimize the experimental conditions, increase the sample size, and further investigate the mechanisms of different molecules in BCC to provide a basis for clinical treatment. The limitations of this study primarily stem from its relatively small sample size and lack of multi-center clinical validation. Although we identified significant findings through transcriptomic sequencing and experimental validation, the homogeneity of the cohort may compromise the generalizability of these results. Furthermore, the incomplete consideration of environmental confounders—including patients' lifestyle factors, genetic predispositions, and external exposures affecting immune infiltration—could introduce additional constraints. To address these limitations, subsequent studies should prioritize expanding cohort sizes and conducting multi-center validations across diverse populations to enhance the reliability and clinical applicability of the findings.

5 Conclusions

This study combined bioinformatics with experimental validation to identify potential gene biomarkers associated with immune cell infiltration in basal cell carcinoma, providing valuable insights for early diagnosis and immunotherapy. These findings underscore the potential application of these biomarkers in precision medicine. qPCR and Western blot analyses revealed that LEF1 and LGR5 were significantly overexpressed in BCC, indicating their promise as novel biomarkers. While the qPCR results indicated an increase in SOX4 expression in BCC, the Western blot analysis did not reveal significant differences in SOX4 protein levels. This inconsistency may stem from factors such as antibody selection, variations in experimental conditions, or low protein levels, highlighting the necessity for further investigation. Preliminary experimental findings suggest that LEF1, LGR5, and SOX4 are likely closely associated with the development of BCC and may serve as promising biomarkers. However, further studies are essential to refine the experimental conditions, expand the sample size, and conduct comprehensive validation to evaluate the potential applications of these biomarkers in the diagnosis and treatment of BCC.

Acknowledgements We sincerely thank the public databases, including TCGA, GEO, HPA, STRING plotter and www.xiantao.love, for providing open access.We acknowledge and appreciate our colleagues for their valuable suggestions and technical assistance for this study.

Author contributions Pengfei Fan and Yun Liu are co-first authors and contributed equally to the study design, data collection, data analysis, experiment execution, and creation and revision of the manuscript. Lei Li (corresponding author) was responsible for the overall research design, funding acquisition, project coordination, guiding the experimental process, supervising data analysis and provided substantial support in writing, revising, and submitting the manuscript. Lei Li also handled the manuscript submission, the peer review process, and all communication with the journal. Tengxiao Ma participated in the experimental design and data collection, provided technical support for data analysis, and assisted in writing parts of the manuscript. Qiaoxing Wang was responsible for data organization and analysis, assisted in the literature review and data presentation, and contributed to writing and editing parts of the manuscript.

Funding This study was supported by Education Department of Hainan Province,China [grant numbers Hnky2025ZC-5] and Hainan Medical University,China [grant numbers S202411810029].

Data availability The data described in this Data Note can be freely and openly accessed on [Name of data depository] under [Identifier, DOI, accession number etc.]. Please see Table 1 and references [Reference numbers] for details and links to the data.

Declarations

Ethics approval and consent to participate The studies involving human tissue specimens were reviewed and approved by the Ethical Review Committee of Hainan Affiliated Hospital of Hainan Medical University. The patients/participants provided written informed consent to participate in this study. Written informed consent was obtained from the individual(s) for the publication of any potentially identifiable images or data included in this article.

Consent for publication Not applicable.

Competing interests The authors declare no competing interests.

References

1. Verkouteren J, Ramdas K, Wakkee M, Nijsten T. Epidemiology of basal cell carcinoma: scholarly review. Br J Dermatol. 2017;177(2):359–72.
2. Madan V, Lear JT, Szeimies R. Non-melanoma skin cancer. The Lancet. 2010;375(9715):673–85.
3. Skin Cancer Foundation-Basal Cell Carcinoma Overview. 2024. https://www.skincancer.org/skin-cancer-information/basal-cell-carcinoma/
4. Naik PP, Desai MB. Basal cell carcinoma: a narrative review on contemporary diagnosis and management. Oncol Ther. 2022;10(2):317–35.
5. Teng Y, Yu Y, Li S, Huang Y, Xu D, Tao X, Fan Y, et al. Ultraviolet radiation and basal cell carcinoma: an environmental perspective. Front Public Health. 2021;9:666528.
6. Christenson LJ, Borrowman TA, Vachon CM, Tollefson MM, Otley CC, Weaver AL, Roenigk RK, et al. Incidence of basal cell and squamous cell carcinomas in a population younger than 40 years. JAMA. 2005;294(6):681–90.
7. Brash DE, Rudolph JA, Simon JA, Lin A, McKenna GJ, Baden HP, Ponten J, et al. A role for sunlight in skin cancer: UV-induced p53 mutations in squamous cell carcinoma. Proc Natl Acad Sci U S A. 1991;88(22):10124–8.
8. Fania L, Didona D, Morese R, Campana I, Coco V, Di Pietro FR, Ricci F, Pallotta S, Candi E, Abeni D, Dellambra E. Basal Cell Carcinoma: From Pathophysiology to Novel Therapeutic Approaches. Biomedicines. 2020 Oct 23;8(11):449,1–38.
9. Snaidr VA, Damian DL, Halliday GM. Nicotinamide for photoprotection and skin cancer chemoprevention: a review of efficacy and safety. EXP DERMATOL. 2019;28:15–22.
10. Lomas A, Leonardi-Bee J, Bath-Hextall F. A systematic review of worldwide incidence of nonmelanoma skin cancer. Br J Dermatol. 2012;166(5):1069–80.
11. Goldenberg G, Karagiannis T, Palmer JB, Lotya J, O'Neill C, Kisa R, Siegel DM, et al. Incidence and prevalence of basal cell carcinoma (BCC) and locally advanced BCC (LABCC) in a large commercially insured population in the United States: a retrospective cohort study. J AM ACAD DERMATOL. 2016;75(5):957–66.
12. Peris K, Fargnoli MC, Garbe C, Kaufmann R, Bastholt L, Seguin NB, Grob JJ, et al. Diagnosis and treatment of basal cell carcinoma: European consensus-based interdisciplinary guidelines. EUR J CANCER. 2019;118:10–34.
13. Stratigos AJ, Sekulic A, Peris K, Bechter O, Prey S, Kaatz M, Fury MG, et al. Cemiplimab in locally advanced basal cell carcinoma after hedgehog inhibitor therapy: an open-label, multi-centre, single-arm, phase 2 trial. LANCET ONCOL. 2021;22(6):848–57.

14. Ramelyte E, Restivo G, Mannino M, Levesque MP, Dummer R. Advances in the drug management of basal cell carcinoma. Expert Opin Pharmacother. 2022;23(5):573–82.
15. Kilgour JM, Jia JL, Sarin KY. Review of the molecular genetics of basal cell carcinoma; inherited susceptibility, somatic mutations, and targeted therapeutics. Cancers (Basel). 2021;13(15):3870,1–16.
16. Bakshi A, Chaudhary SC, Rana M, Elmets CA, Athar M. Basal cell carcinoma pathogenesis and therapy involving hedgehog signaling and beyond. Mol Carcinog. 2017;56(12):2543–57.
17. Genetics of Skin Cancer (PDQ(R)): Health Professional Version. 2002. https://www.cancer.gov/types/skin/hp/skin-genetics-pdq
18. Pellegrini C, Maturo MG, Di Nardo L, Ciciarelli V, Gutierrez GC, Fargnoli MC. Understanding the molecular genetics of basal cell carcinoma. Int J Mol Sci. 2017;18(11):2485:1–16.
19. Altaraihi M, Wadt K, Ek J, Gerdes AM, Ostergaard E. A healthy individual with a homozygous PTCH2 frameshift variant: are variants of PTCH2 associated with nevoid basal cell carcinoma syndrome? Hum Genome Var. 2019;6:10.
20. Arneth B. Tumor microenvironment. Medicina (Kaunas). 2019;56(1):15:1–21.
21. Grivennikov SI, Greten FR, Karin M. Immunity, inflammation, and cancer. Cell. 2010;140(6):883–99.
22. Amor NG, Santos P, Campanelli AP. The tumor microenvironment in SCC: mechanisms and therapeutic opportunities. Front Cell Dev Biol. 2021;9:636544.
23. Ji AL, Rubin AJ, Thrane K, Jiang S, Reynolds DL, Meyers RM, Khavari PA, et al. Multimodal analysis of composition and spatial architecture in human squamous cell carcinoma. Cell. 2020;182(2):497–514.
24. Amit M, Takahashi H, Dragomir MP, Lindemann A, Gleber-Netto FO, Pickering CR, Myers JN, et al. Loss of p53 drives neuron reprogramming in head and neck cancer. Nature. 2020;578(7795):449–54.
25. Xiao Y, Ma D, Zhao S, Suo C, Shi J, Xue MZ, Shao ZM, et al. Multi-omics profiling reveals distinct microenvironment characterization and suggests immune escape mechanisms of triple-negative breast cancer. Clin Cancer Res. 2019;25(16):5002–14.
26. Perrone M, Talarico G, Chiodoni C, Sangaletti S. Impact of immune cell heterogeneity on HER2+ breast cancer prognosis and response to therapy. Cancers (Basel). 2021;13(24):6352:1–16.
27. Geels SN, Moshensky A, Sousa RS, Murat C, Bustos MA, Walker BL, Marangoni F, et al. Interruption of the intratumor CD8(+) T cell: Treg crosstalk improves the efficacy of PD-1 immunotherapy. Cancer Cell. 2024;42(6):1051–66.
28. Beksac B, Ilter N, Erdem O, Cakmak P, Cenetoglu S, Yapar D. Sparsity of dendritic cells and cytotoxic T cells in tumor microenvironment may lead to recurrence in basal cell carcinoma. INT J DERMATOL. 2020;59(10):1258–63.
29. Omland SH, Wettergren EE, Mollerup S, Asplund M, Mourier T, Hansen AJ, Gniadecki R, et al. Correction to: cancer associated fibroblasts (CAFs) are activated in cutaneous basal cell carcinoma and in the peritumoural skin. BMC Cancer. 2018;18(1):111.
30. Kaporis HG, Guttman-Yassky E, Lowes MA, Haider AS, Fuentes-Duculan J, Darabi K, Carucci JA, et al. Human basal cell carcinoma is associated with Foxp3+ T cells in a Th2 dominant microenvironment. J Invest Dermatol. 2007;127(10):2391–8.
31. Riker AI, Enkemann SA, Fodstad O, Liu S, Ren S, Morris C, Matta J, et al. The gene expression profiles of primary and metastatic melanoma yields a transition point of tumor progression and metastasis. BMC Med Genomics. 2008;1:13.
32. Yunoki T, Tabuchi Y, Hirano T, Miwa S, Imura J, Hayashi A. Gene networks in basal cell carcinoma of the eyelid, analyzed using gene expression profiling. Oncol Lett. 2018;16(5):6729–34.
33. Ning H, Mitsui H, Wang CQ, Suarez-Farinas M, Gonzalez J, Shah KR, Krueger JG, et al. Identification of anaplastic lymphoma kinase as a potential therapeutic target in Basal Cell Carcinoma. Oncotarget. 2013;4(12):2237–48.
34. Wan J, Dai H, Zhang X, Liu S, Lin Y, Somani AK, Han J, et al. Distinct transcriptomic landscapes of cutaneous basal cell carcinomas and squamous cell carcinomas. Genes Dis. 2021;8(2):181–92.
35. Ginestet C. ggplot2: elegant graphics for data analysis. J Roy Stat Soc. 2011;174(1):245–6.
36. Ritchie ME, Phipson B, Wu D, Hu Y, Law CW, Shi W, Smyth GK, et al. limma powers differential expression analyses for RNA-sequencing and microarray studies. Nucleic Acids Res. 2015;43(7):e47.
37. Gu Z, Eils R, Schlesner M. Complex heatmaps reveal patterns and correlations in multidimensional genomic data. Bioinformatics. 2016;32(18):2847–9.
38. Hanzelmann S, Castelo R, Guinney J. GSVA: gene set variation analysis for microarray and RNA-seq data. BMC Bioinform. 2013;14:7.
39. Bindea G, Mlecnik B, Tosolini M, Kirilovsky A, Waldner M, Obenauf AC, Galon J, et al. Spatiotemporal dynamics of intratumoral immune cells reveal the immune landscape in human cancer. Immunity. 2013;39(4):782–95.
40. Asgari MM, Moffet HH, Ray GT, Quesenberry CP. Trends in basal cell carcinoma incidence and identification of high-risk subgroups, 1998–2012. JAMA DERMATOL. 2015;151(9):976–81.
41. Leiter U, Keim U, Garbe C. Epidemiology of skin cancer: update 2019. Adv Exp Med Biol. 2020;1268:123–39.
42. Sekulic A, Migden MR, Oro AE, Dirix L, Lewis KD, Hainsworth JD, Hauschild A, et al. Efficacy and safety of vismodegib in advanced basal-cell carcinoma. N Engl J Med. 2012;366(23):2171–9.
43. Liang J, Li Y, Daniels G, Sfanos K, De Marzo A, Wei J, Lee P, et al. LEF1 targeting EMT in prostate cancer invasion is regulated by miR-34a. Mol Cancer Res. 2015;13(4):681–8.
44. Freihen V, Ronsch K, Mastroianni J, Frey P, Rose K, Boerries M, Hecht A, et al. SNAIL1 employs beta-Catenin-LEF1 complexes to control colorectal cancer cell invasion and proliferation. Int J Cancer. 2020;146(8):2229–42.
45. Kim GH, Fang XQ, Lim WJ, Park J, Kang TB, Kim JH, Lim JH, et al. Cinobufagin suppresses melanoma cell growth by inhibiting LEF1. Int J Mol Sci. 2020;21(18):6706:1–13.
46. Qi Y, Shan Y, Li S, Huang Y, Guo Y, Huang T, Jia L, et al. LncRNA LEF1-AS1/LEF1/FUT8 axis mediates colorectal cancer progression by regulating alpha1, 6-fucosylationvia Wnt/beta-catenin pathway. Dig Dis Sci. 2022;67(6):2182–94.
47. Zhang Z, Kim K, Li X, Moreno M, Sharp T, Goodheart MJ, Amendt BA, et al. MicroRNA-26b represses colon cancer cell proliferation by inhibiting lymphoid enhancer factor 1 expression. Mol Cancer Ther. 2014;13(7):1942–51.
48. Selvakumar SC, Preethi KA, Sekar D. MicroRNA-510-3p regulated vascular dysfunction in preeclampsia by targeting vascular endothelial growth factor A (VEGFA) and its signaling axis. Placenta. 2024;153:31–52.
49. Selvakumar SC, Preethi KA, Sekar D. MicroRNAs as important players in regulating cancer through PTEN/PI3K/AKT signalling pathways. Biochim Biophys Acta Rev Cancer. 2023;1878(3):188904.

50. Chen HC, Mueller N, Stott K, Kapeni C, Rivers E, Sauer CM, de la Roche M, et al. Publisher correction: novel immunotherapeutics against LGR5 to target multiple cancer types. EMBO MOL MED. 2024;16(11):3026.
51. Shimokawa M, Ohta Y, Nishikori S, Matano M, Takano A, Fujii M, Sato T, et al. Visualization and targeting of LGR5(+) human colon cancer stem cells. Nature. 2017;545(7653):187–92.
52. Xu L, Lin W, Wen L, Li G. Lgr5 in cancer biology: functional identification of Lgr5 in cancer progression and potential opportunities for novel therapy. Stem Cell Res Ther. 2019;10(1):219.
53. Zhang S, Kim K, Jin UH, Pfent C, Cao H, Amendt B, Safe S, et al. Aryl hydrocarbon receptor agonists induce microRNA-335 expression and inhibit lung metastasis of estrogen receptor negative breast cancer cells. Mol Cancer Ther. 2012;11(1):108–18.
54. Leone P, Berardi S, Frassanito MA, Ria R, De Re V, Cicco S, Racanelli V, et al. Dendritic cells accumulate in the bone marrow of myeloma patients where they protect tumor plasma cells from CD8+ T-cell killing. Blood. 2015;126(12):1443–51.
55. Besnard AG, Guabiraba R, Niedbala W, Palomo J, Reverchon F, Shaw TN, Liew FY, et al. IL-33-mediated protection against experimental cerebral malaria is linked to induction of type 2 innate lymphoid cells, M2 macrophages and regulatory T cells. PLOS PATHOG. 2015;11(2):e1004607.
56. Haeberle S, Raker V, Haub J, Kim YO, Weng SY, Yilmaz OK, Hadaschik EN, et al. Regulatory T cell deficient scurfy mice exhibit a Th2/M2-like inflammatory response in the skin. J Dermatol Sci. 2017;87(3):285–91.
57. Liu XS, Lin XK, Mei Y, Ahmad S, Yan CX, Jin HL, Yu JR, et al. Regulatory T cells promote overexpression of Lgr5 on gastric cancer cells via TGF-beta1 and confer poor prognosis in gastric cancer. Front Immunol. 2019;10:1741.
58. Geng X, Li M, Cui B, Lu C, Liu X, Zhang P, Lu Z, et al. CD4+CD25+Foxp3+ regulatory T cells suppress NKG2D-mediated NK cell cytotoxicity in peripheral blood. Medicine (Baltimore). 2019;98(22):e15722.
59. Ohira K, Nakahara A, Konnai S, Okagawa T, Nishimori A, Maekawa N, Ohashi K, et al. Bovine leukemia virus reduces anti-viral cytokine activities and NK cytotoxicity by inducing TGF-beta secretion from regulatory T cells. Immun Inflamm Dis. 2016;4(1):52–63.
60. Wang Z, Guo L, Song Y, Zhang Y, Lin D, Hu B, Liu H, et al. Augmented anti-tumor activity of NK-92 cells expressing chimeric receptors of TGF-betaR II and NKG2D. Cancer Immunol Immunother. 2017;66(4):537–48.
61. Liu X, Wang C, Zhang X, Zhang R. LEF1 is associated with immunosuppressive microenvironment of patients with lung adenocarcinoma. Medicine (Baltimore). 2024;103(41):e39892.
62. Hodkinson BP, Schaffer M, Brody JD, Jurczak W, Carpio C, Ben-Yehuda D, Balasubramanian S, et al. Biomarkers of response to ibrutinib plus nivolumab in relapsed diffuse large B-cell lymphoma, follicular lymphoma, or Richter's transformation. Transl Oncol. 2021;14(1):100977.
63. Zhao P, Sun L, Zhao C, Malik S. PD1 is transcriptionally regulated by LEF1 in mature T cells. Immunobiology. 2023;228(5):152708.